JOURNAL OF THEORETICAL AND APPLIED MECHANICS
48, 3, pp. 813-837, Warsaw 2010

UNDESIDERED DRIFT OF MULTIBODY MODELS EXCITED BY MEASURED ACCELERATIONS OR FORCES[1]

Michael Speckert
Nikolaus Ruf
Klaus Dressler

Fraunhofer Institute for Industrial Mathematics, Kaiserslautern, Germany
e-mail: michael.speckert@itwm.fraunhofer.de

In the ground vehicle industry, it is important to simulate multibody models of the full vehicle based on wheel forces and moments in order to derive section forces at certain components for durability assessment. This is difficult due to noise in the input data and the unavoidable deviation between the model and real vehicle. Both lead to an undesired drift of the vehicle model in the simulation. This paper shortly describes the sources of these effects and shows that, due to missing knowledge about the true trajectory of the vehicle, this problem cannot be solved by an improved numerical treatment of the underlying equations. Several ways to deal with the problem are briefly reported. Finally, a simple vehicle model is used to show all the effects.

Key words: multibody simulation, full vehicle model, force-based simulation, drift due to noise

1. Introduction

In the ground vehicle industry, measurements on vehicles driving over test tracks or public roads are performed in order to derive loads for test rigs or numerical verification. Often 100-200 different quantities at different spots of the vehicle are measured, among which we have wheel forces (measured at the hub), spring displacements, strains, or accelerations. The data can be used either for directly setting up rig tests for certain components or for the excitation of multibody models of the vehicle in order to calculate section forces.

[1]The paper was presented at the ECCOMAS Thematic Conference on *Multibody Dynamics* which was held at Warsaw University of Technology on June 29 – July 2, 2009.

Besides the 'internal' excitation of the vehicle by steering, acceleration, or braking, the main 'external' excitation is given by the forces at the contact patches between tyres and ground. These are reaction forces which in principle can be computed based on a digitised road profile, a tyre model as a part of the vehicle model, and a driver model driving the vehicle. However, this approach requires accurate tyre models as well as the digitised road and the driver. An alternative way of exciting the full vehicle model is to virtually cut off the tyres and use measured wheel forces as input.

While simulating such an unconstrained system based on section forces is very important in practice, it is difficult due to noise in the input data and the unavoidable deviation between the model and real vehicle. This leads to an undesired drift of the vehicle, which can be explained by the theory of stochastic differential equations. Additional measurements are needed to circumvent such problems. Typically, measured accelerations of the vehicle body exist, but these alone do not help. Instead, data on the velocity or even displacement level are needed to deal with the drift.

In Section 2, the drift due to noisy input data during integration is studied using the most basic example of a point mass subject to a force. In Section 3, some investigations on how to circumvent the drift are reported. Finally, in Section 4, we use a model of a simple demonstration vehicle to exemplify the theoretical considerations.

2. Integration of noisy data

In this section, we study a simple differential equation to illustrate the problems inherent in integrating noisy data. We make use of some basic results from stochastic analysis but do not treat them in great detail, as this is not the main focus of this paper. A brief introduction to the theory of stochastic differential equations (SDEs) with applications can be found in Kloeden *et al.* (2002).

As an example, we consider the one-dimensional equation of motion for a point mass

$$dx = v\,dt \qquad dv = \Big(\frac{f}{m} - \eta v\Big)\,dt \qquad x(0) = v(0) = 0 \tag{2.1}$$

This ODE describes the velocity $v(t)$ and position $x(t)$ of an object with a mass $m > 0$ subject to the accelerating force $f(t)$, provided the object was at rest at the time $t = 0$. The damping term (friction) proportional to the velocity is also included, with damping constant $\eta \geqslant 0$.

The problem now is to reconstruct the velocity and position based on measurements distorted by unsystematic errors which we model as independent Gaussian random variables. If we denote the time step between observations by Δt, the forces we actually observe are

$$\widetilde{f}(n\Delta t) \sim \mathrm{N}\,(f(n\Delta t), \sigma_M^2) \tag{2.2}$$

with some variance $\sigma_M^2 > 0$ representing the accuracy of the measurement device. The impact of the noise on the reconstructed velocity and position depends on the discretisation scheme we have chosen to solve (2.1). We use the explicit Euler scheme for our example, as it permits us to study error propagation in terms of a simple SDE. To derive it, we begin with the difference equation for the velocity, taking the time step to be equal to the rate of observations

$$\begin{aligned} &\widetilde{v}_{n+1} := \widetilde{v}((n+1)\Delta t) := \widetilde{v}_n + \Big(\frac{f(n\Delta t) + \epsilon_n}{m} - \eta\widetilde{v}_n\Big)\Delta t \\ &\widetilde{v}_0 := \widetilde{v}(0) := 0 \end{aligned} \tag{2.3}$$

The errors ϵ_n are i.i.d. Gaussian random variables with mean zero and variance σ_M^2. If the true force is L^2-integrable and Δt sufficiently small, a solution to the difference equation approximates the solution to the following Itô-SDE on the discrete time grid given by Δt

$$\begin{aligned} &d\widetilde{x} = \widetilde{v}\,dt \qquad\qquad d\widetilde{v} = \Big(\frac{f}{m} - \eta\widetilde{v}\Big)dt + \frac{\sigma}{m}dW(t) \\ &\widetilde{x}(0) = \widetilde{v}(0) = 0 \end{aligned} \tag{2.4}$$

To determine the variance σ^2 of the Brownian motion in the limiting case, we note that the variance of the increments is

$$\mathrm{Var}\,(\epsilon_n \Delta t) = \sigma_M^2 (\Delta t)^2 \stackrel{!}{=} \sigma^2 \Delta t \quad\Longleftrightarrow\quad \sigma^2 = \sigma_M^2 \Delta t \tag{2.5}$$

We have seen that if we solve ODE (2.1) with perturbed forces using the explicit Euler scheme, what we actually do is construct a path of the solution to SDE (2.4). Its usefulness for the purpose of simulation depends on how far it deviates from the actual values. As the individual errors have bounded variance, we might hope that $\widetilde{v}$ and $\widetilde{x}$ share this property. Unfortunately, this is only true for the velocity, and only if the damping constant η is positive.

The unique solution to (2.1) is

$$x(t) = \int_0^t v(s)\,ds \qquad\qquad v(t) = \frac{1}{m}\int_0^t \mathrm{e}^{\eta(s-t)} f(s)\,ds \tag{2.6}$$

For SDE (2.4), we distinguish two cases

(1) No damping: If $\eta = 0$, the solution is

$$\widetilde{x}(t) = x(t) + \frac{\sigma}{m}\int_0^t W(s)\,ds \qquad \widetilde{v}(t) = v(t) + \frac{\sigma}{m}W(t) \tag{2.7}$$

The integrated Brownian motion has mean zero and variance $t^3/3$, meaning that the expectation and variance of the solutions are

$$\begin{aligned} \mathrm{E}\,(\widetilde{x}(t)) &= x(t) & \mathrm{Var}\,(\widetilde{x}(t)) &= \frac{\sigma^2 t^3}{3m^2} \\ \mathrm{E}\,(\widetilde{v}(t)) &= v(t) & \mathrm{Var}\,(\widetilde{v}(t)) &= \frac{\sigma^2 t}{m^2} \end{aligned} \tag{2.8}$$

While the stochastic process is centered around the true solution, its variance grows to infinity as time progresses. As a measure of the error growth, we use the standard deviation, since it is proportional to the width of the confidence interval for the Gaussian process around its mean

$$\mathrm{Std}\,(\widetilde{v}(t)) = O(t^{\frac{1}{2}}) \qquad \mathrm{Std}\,(\widetilde{x}(t)) = O(t^{\frac{3}{2}}) \tag{2.9}$$

(2) Damping: For $\eta > 0$, we obtain

$$\begin{aligned} \widetilde{x}(t) &= x(t) + \frac{\sigma}{\eta m}\Big(W(t) - \int_0^t \mathrm{e}^{\eta(s-t)}\,dW(s)\Big) \\ \widetilde{v}(t) &= v(t) + \frac{\sigma}{m}\int_0^t \mathrm{e}^{\eta(s-t)}\,dW(s) \end{aligned} \tag{2.10}$$

In this case, the velocity consists of a deterministic trend and an Ornstein-Uhlenbeck (mean reversal) process with mean 0. As the latter has bounded variance, the reconstruction of v is merely a question of how accurate the initial measurements are. Unfortunately, the variance of the position is once again unbounded although it grows more slowly than in the undampened case

$$\begin{aligned} &\mathrm{E}\,(\widetilde{x}(t)) = x(t) \\ &\mathrm{Var}\,(\widetilde{x}(t)) = \frac{\sigma^2}{\eta^2 m^2}\Big(t + \frac{1-\mathrm{e}^{-2\eta t}}{2\eta} - \frac{2(1-\mathrm{e}^{-\eta t})}{\eta}\Big) \\ &\mathrm{E}\,(\widetilde{v}(t)) = v(t) \qquad \mathrm{Var}\,(\widetilde{v}(t)) = \frac{\sigma^2}{2\eta m^2}(1-\mathrm{e}^{-2\eta t}) \end{aligned} \tag{2.11}$$

Here, we have used the Itô-isometry to calculate

$$\mathrm{Var}\left(\int_0^t \mathrm{e}^{\eta(s-t)}\, dW(s)\right) = \mathrm{E}\left(\left(\int_0^t \mathrm{e}^{\eta(s-t)}\, dW(s)\right)^2\right) = \frac{1-\mathrm{e}^{-2\eta t}}{2\eta} \tag{2.12}$$

To evaluate the variance of $\widetilde{x}(t)$, we also need

$$\mathrm{Cov}\left(W(t), \int_0^t \mathrm{e}^{\eta(s-t)}\, dW(s)\right) = \mathrm{E}\left(W(t)\int_0^t \mathrm{e}^{\eta(s-t)}\, dW(s)\right) = \frac{1-\mathrm{e}^{-\eta t}}{\eta} \tag{2.13}$$

where we use the product rule of Itô-calculus to evaluate the product, dropping all stochastic terms as they have the mean zero.

In the presence of damping, the standard deviations grow with time as

$$\mathrm{Std}\,(\widetilde{v}(t)) = O(1) \qquad \mathrm{Std}\,(\widetilde{x}(t)) = O(t^{\frac{1}{2}}) \tag{2.14}$$

We have seen that even for simple model (2.1), a stable (bounded variance) solution exists only if we integrate but once and include a correction term in the equations. Integrating twice will always lead to errors that grow progressively larger over time. The situation can only get worse for a problem involving several bodies, as their relative position and orientation is progressively distorted. This leads to spurious interaction forces and gravity acting in the wrong direction.

It should be noted that the problems caused by noise integration are of principal nature, as there is no way to reconstruct the true forces from the measurements. Preprocessing (e.g. smoothing the data) or more sophisticated integration schemes can reduce the variance σ^2, but this only serves to rescale the error, not bound it.

3. Drift correction

In this section, we describe some possible solutions to the drift problem. We consider the case of full vehicle simulation which is needed to derive section forces for certain components. The model is unconstrained and excited by measured wheel forces which are always noisy to some extent. Thus, we have to be aware of the drift of the vehicle body due to the 'Brownian motion effect' described above. Another reason for observing the drift is the fact that the

numerical model is only an approximation of the real vehicle. If, for example, the total mass of the model is too small, then it will lift off during simulation. While the measured wheel forces (up to measurement noise) are 'in equilibrium' with the real vehicle and its motion, this fact need not be true for the numerical model.

First we perform the simulation while ignoring a possible drift and subsequently check the motion of the model. If the observed drift is such that the section forces can be regarded as sufficiently accurate, we are done. This is the case if we have a drift in the translational degrees of freedom only. If the drift of the pitch angle (rotation about the lateral axis) and the roll angle (rotation about the longitudinal axis) is too large, we have to assume that the simulation results are falsified and reject them. We consider the following approaches to deal with the drift:

1. **Artificially constraining the model:** For a vehicle driving over a (possibly rough) horizontal road, we can assume that the pitch and roll angles are small. Thus, we apply a correction to the simulation as soon as the angles become too large. Sometimes this is accomplished by attaching a rotational spring between the vehicle body and ground which always tries to keep the angles close to zero. While this is a simple workaround, it is not clear how to choose the spring parameters and undesired reaction torques are induced. The size of these reaction torques can be taken as a measure of validity of this approach: the larger the torques, the more doubtful the results. Of course, this approach does not help at all if the assumption of the "horizontal road" is not guaranteed, i.e. if we need to simulate curvy, hilly, or even off-road driving.

2. **Additional acceleration sensors:** We use sensors to measure the accelerations at different spots of the vehicle body. This is rather cheap and convenient. These accelerations are used to estimate the motion of the body prior to the simulation. Again, we only need to estimate the orientation (rotational degrees of freedom). The approach is described in more detail in Sec. 3.1 below. As we will see, it does not fully solve the drift problem (since two integration steps are needed here too) such that we have to consider measuring quantities at the velocity or even position level.

3. **Additional measurements on the velocity or position levels:** Since both approaches above are not fully satisfying, we have to introduce additional measurements of either (angular) velocities or angles. If the angles of the vehicle body can be measured, we can guide it during the

simulation to prevent the drift. If only angular velocities can be measured, we still have to perform one integration to get the angles such that we have to expect small drifts. Sec. 3.2 gives some details of that approach.

3.1. Calculating the rigid body motion from measured accelerations

Here, we investigate how to calculate the body motion of a vehicle from measured accelerations. We assume that there are $m+1$, $m \geqslant 3$ sensors at different positions on the body and introduce the following notation:

$\boldsymbol{x}_C, \boldsymbol{x}_i$	–	positions of the reference point C and of the sensors i of the body given in a fixed reference (global frame),
$\mathbf{S}$	–	transformation from the local to global frame. This is the body's orientation in the global frame,
$\boldsymbol{\omega}, \boldsymbol{\omega}_l$	–	angular velocity in the global and local frame,
$\boldsymbol{r}_i$	–	positions of the sensors in the local frame, $i = 1, \ldots, m+1$,
$\boldsymbol{a}_i$	–	measured accelerations at positions $\boldsymbol{x}_i$, $i = 1, \ldots, m+1$,
$\widetilde{\boldsymbol{a}}_i$	–	accelerations at positions $\boldsymbol{x}_i$ in the local frame, $i = 1, \ldots, m+1$,
$\mathbf{A}$	–	matrix of the local relative accelerations, $\mathbf{A} = [\boldsymbol{a}_1 - \boldsymbol{a}_{m+1}, \ldots, \boldsymbol{a}_m - \boldsymbol{a}_{m+1}]$
$\mathbf{R}$	–	matrix of the local relative coordinates, $\mathbf{R} = [\boldsymbol{r}_1 - \boldsymbol{r}_{m+1}, \ldots, \boldsymbol{r}_m - \boldsymbol{r}_{m+1}]$.

With these notations, we have

$$\boldsymbol{x}_i = \boldsymbol{x}_C + \mathbf{S}\boldsymbol{r}_i \qquad i = 1, \ldots, m+1 \tag{3.1}$$

This relation is true only if the body is rigid. Otherwise, we would have to add the deformations. Differentiation and transformation into the local frame gives

$$\widetilde{\boldsymbol{a}}_i = \mathbf{S}^\top \ddot{\boldsymbol{x}}_i = \mathbf{S}^\top \ddot{\boldsymbol{x}}_C + \mathbf{S}^\top \ddot{\mathbf{S}} \boldsymbol{r}_i \qquad i = 1, \ldots, m+1 \tag{3.2}$$

By calculating the relative accelerations we eliminate the translational motion and get $\widetilde{\boldsymbol{a}}_i - \widetilde{\boldsymbol{a}}_{m+1} = \mathbf{S}^\top \ddot{\mathbf{S}}(\boldsymbol{r}_i - \boldsymbol{r}_{m+1})$, $i = 1, \ldots, m$. Usually, the sensors are performing a correction with respect to gravity. Since the orientation of the sensors during measurement is unknown, the result of the correction is

$$\boldsymbol{a}_i = \widetilde{\boldsymbol{a}}_i + g\boldsymbol{e}_3 - \mathbf{S}^\top g \boldsymbol{e}_3 \qquad i = 1, \ldots, m \tag{3.3}$$

where g denotes the gravitational constant and $\boldsymbol{e}_3$ denotes the direction of gravity (global z-coordinate). For the relative accelerations $\boldsymbol{a}_i - \boldsymbol{a}_{m+1}$ this correction term cancels and we get $\mathbf{A} = \mathbf{S}^\top \ddot{\mathbf{S}} \mathbf{R}$. The matrices $\mathbf{R}$ and $\mathbf{A}$ contain

the relative positions and accelerations respectively of the first m sensors with respect to the last one. Since the unknown transformation matrix $\mathbf{S}$ contains only three degrees of freedom (for example Euler or Cardan angles), this matrix equation is an overdetermined set of equations for the three parameters (if $m > 3$). The number of equations depends on the number of sensors. By multiplication with the pseudo inverse (Moore-Penrose inverse) $\mathbf{R}^+$ from the right, we get

$$\mathbf{S}^\top \ddot{\mathbf{S}} = \mathbf{A}\mathbf{R}^+ \tag{3.4}$$

This operation partly removes the redundant accelerations. The remaining equation still contains the inherent consistency condition induced by the fact that the body is non-deformable.

Calculation of the transformation matrix and the angles

By differentiating the identity $\mathbf{I}_3 = \mathbf{S}^\top \mathbf{S}$ we obtain

$$\mathbf{S}^\top \dot{\mathbf{S}} = \widetilde{\boldsymbol{\omega}}_l = \begin{bmatrix} 0 & -\omega_{l,3} & \omega_{l,2} \\ \omega_{l,3} & 0 & -\omega_{l,1} \\ -\omega_{l,2} & \omega_{l,1} & 0 \end{bmatrix} \tag{3.5}$$

where $\boldsymbol{\omega}_l$ denotes the vector of the local angular velocity and $\widetilde{\boldsymbol{\omega}}_l$ is the corresponding skew symmetric matrix. Another differentiation leads to $\mathbf{S}^\top \ddot{\mathbf{S}} = \dot{\widetilde{\boldsymbol{\omega}}}_l - \widetilde{\boldsymbol{\omega}}_l \widetilde{\boldsymbol{\omega}}_l^\top = \dot{\widetilde{\boldsymbol{\omega}}}_l + \widetilde{\boldsymbol{\omega}}_l \widetilde{\boldsymbol{\omega}}_l$, and together with (3.4) we obtain $\dot{\widetilde{\boldsymbol{\omega}}}_l + \widetilde{\boldsymbol{\omega}}_l \widetilde{\boldsymbol{\omega}}_l = \mathbf{S}^\top \ddot{\mathbf{S}} = \mathbf{A}\mathbf{R}^+ =: \mathbf{M}$. Since $\dot{\widetilde{\boldsymbol{\omega}}}_l$ is skew symmetric and the product $\widetilde{\boldsymbol{\omega}}_l \widetilde{\boldsymbol{\omega}}_l$ is symmetric, we have a decomposition of the left-hand side of this equation into the symmetric and skew symmetric part. Thus, if we define

$$\mathbf{M}_- = \frac{1}{2}[\mathbf{A}\mathbf{R}^+ - (\mathbf{A}\mathbf{R}^+)^\top] \qquad \mathbf{M}_+ = \frac{1}{2}[\mathbf{A}\mathbf{R}^+ + (\mathbf{A}\mathbf{R}^+)^\top]$$

we arrive at

$$\dot{\widetilde{\boldsymbol{\omega}}}_l = \mathbf{M}_- \qquad \widetilde{\boldsymbol{\omega}}_l \widetilde{\boldsymbol{\omega}}_l = \mathbf{M}_+ \tag{3.6}$$

The first of these relations is a simple set of three uncoupled equations for the local angular velocities and the second one is the consistency condition mentioned above. The transition from $\mathbf{A}$ and $\mathbf{R}^+$ to $\mathbf{M}_-$ can be interpreted as a projection onto the rigid body motion. Due to possible measurement errors and the deviation from the rigid body motion, we have to take into account large uncertainties in $\mathbf{M}_-$. Using (3.6) we obtain $\boldsymbol{\omega}_l$ by simple integration. Of course, during integration we have to deal with the accumulation of random errors leading to a drift.

The next step is to calculate the transformation matrix $\mathbf{S}$ from the local angular velocities $\boldsymbol{\omega}_l$. To this end, we write $\mathbf{S}$ using quaternions in the form

$$\mathbf{S} = \mathbf{S}(\boldsymbol{q}) = \begin{bmatrix} q_1^2+q_2^2-q_3^2-q_4^2 & 2(q_2q_3-q_1q_4) & 2(q_2q_4+q_1q_3) \\ 2(q_2q_3+q_1q_4) & q_1^2-q_2^2+q_3^2-q_4^2 & 2(q_3q_4-q_1q_2) \\ 2(q_2q_4-q_1q_3) & 2(q_3q_4+q_1q_2) & q_1^2-q_2^2-q_3^2+q_4^2 \end{bmatrix} \tag{3.7}$$

where $\boldsymbol{q} = [q_1, q_2, q_3, q_4]^\top$ and $\|\boldsymbol{q}\|^2 = q_1^2+q_2^2+q_3^2+q_4^2 = 1$. Using (3.5), we arrive at the linear system of equations

$$\begin{aligned} \dot{\boldsymbol{q}} &= \frac{1}{2}\boldsymbol{\Omega}_l\boldsymbol{q} \\ \boldsymbol{\Omega}_l &= \left[\begin{array}{c|ccc} 0 & -\omega_{l,1} & -\omega_{l,2} & -\omega_{l,3} \\ \hline \omega_{l,1} & 0 & \omega_{l,3} & -\omega_{l,2} \\ \omega_{l,2} & -\omega_{l,3} & 0 & \omega_{l,1} \\ \omega_{l,3} & \omega_{l,2} & -\omega_{l,1} & 0 \end{array}\right] = \left[\begin{array}{c|c} 0 & -\boldsymbol{\omega}_l \\ \hline \boldsymbol{\omega}_l & -\widetilde{\boldsymbol{\omega}}_l \end{array}\right] \end{aligned} \tag{3.8}$$

for the quaternions $\boldsymbol{q}$. Since $\boldsymbol{\Omega}_l$ is skew symmetric, the normalisation $\|\boldsymbol{q}\|^2 = 1$ is preserved during integration. In contrast to other representations of the transformation matrix (Euler or Cardan angles), (3.8) does not contain singularities and can be integrated over the desired period.

Calculation of the body position

Once the angles α resp. the transformation matrix $\mathbf{S}$ are known, we can calculate the body position $\boldsymbol{x}_C$. Combining (3.2) and (3.3), we get

$$\ddot{\boldsymbol{x}}_C = \mathbf{S}\widetilde{\boldsymbol{a}}_i - \ddot{\mathbf{S}}\boldsymbol{r}_i = \mathbf{S}(\boldsymbol{a}_i - g\boldsymbol{e}_3) + g\boldsymbol{e}_3 - \ddot{\mathbf{S}}\boldsymbol{r}_i \qquad i = 1, \ldots, m+1$$

To minimise errors, we calculate the average acceleration

$$\ddot{\overline{\boldsymbol{x}}}_C = \frac{1}{m+1}\sum_{i=1}^{m+1}[\mathbf{S}(\boldsymbol{a}_i - g\boldsymbol{e}_3) + g\boldsymbol{e}_3 - \ddot{\mathbf{S}}\boldsymbol{r}_i] \tag{3.9}$$

Integrating twice leads to the position $\boldsymbol{x}_C$. Of course, we will again have a drift during the integration of $\ddot{\overline{\boldsymbol{x}}}_C$. The remaining positions $\boldsymbol{x}_i$ follow from (3.1).

Summary

The process of calculating the position and orientation of the body from the measured accelerations can be summarised as follows:

1. Calculate the matrix $\mathbf{M}_- = 0.5[\mathbf{A}\mathbf{R}^+ - (\mathbf{A}\mathbf{R}^+)^\top]$.
2. Calculate the local angular velocity by integration of $\dot{\tilde{\boldsymbol{\omega}}}_l = \mathbf{M}_-$.
3. Calculate the quaternions $\boldsymbol{q}$ by integration of $\dot{\boldsymbol{q}} = 0.5\boldsymbol{\Omega}_l\boldsymbol{q}$.
4. Calculate the transformation matrix $\mathbf{S}$ from (3.7).
5. Calculate $\ddot{\boldsymbol{x}}_C$ according to (3.9) and $\boldsymbol{x}_C$ by twofold integration.
6. Calculate the remaining positions $\boldsymbol{x}_i$ according to (3.1).

Remarks

1. Having calculated the transformation matrix $\mathbf{S}$, a convenient parametrisation, e.g. Euler or Cardan angles, can be derived.
2. The calculation of the local angular velocities $\boldsymbol{\omega}_l$ by integration of $\dot{\tilde{\boldsymbol{\omega}}}_l = \mathbf{M}_-$ is the most critical step since the right hand side $\mathbf{M}_-$ is disturbed by measurement errors and the fact that the car body is not really rigid. Thus, we have to expect a drift in $\boldsymbol{\omega}_l$. If the real vehicle motion during measuring is such that the angular velocities as well as the angles have mean zero and no drift, we can apply a high pass filter to $\boldsymbol{\omega}_l$ prior to solving $\dot{\boldsymbol{q}} = 0.5\boldsymbol{\Omega}_l\boldsymbol{q}$ and again apply a high pass filter to the resulting angles α. However, the final results will depend on the filter parameters (cut-off frequency) and the best choice of parameters is subjective.
3. With this approach (just like the "big spring constraint") we still cannot objectively distinguish the undesired angular drift from angular movement that may come from a curvy or hilly road.
4. A direct measurement of the angular velocities would be much more reliable. The same remarks apply to the calculation of the position by twofold integration of $\ddot{\boldsymbol{x}}_C$. Again we can apply high pass filtering, but the parameter choice is subjective.
5. Nevertheless, the algorithm establishes the relation between the vehicle body motion and accelerations in a rigorous way and, at least, enables the estimation of motion in case no additional measurements are available.

3.2. Measurement of angular velocities or angles

We have already argued that for the purpose of calculating section forces, the errors in the position of the vehicle are negligible, while its orientation with respect to gravity must be known with sufficient accuracy. An obvious way to improve the quality of simulation is thus to include measured angles. Typically, these are determined by an inertial navigation system (INS) on board the

vehicle. Since an INS uses gyroscopes for measuring angular velocities, any angles reported are derived via integration.

As in Sec. 2, we model the noise on the angular velocities as a Brownian motion with variance $\sigma^2 > 0$. The angular velocities in the local reference frame are replaced by

$$\omega_{l,j} \to \omega_{l,j} + \sigma \, dW_j(t) \tag{3.10}$$

with independent Brownian motions W_j. Now, quaternion representation (3.7) yields the following SDE

$$\begin{aligned} d\widetilde{\boldsymbol{q}} &= \frac{1}{2}\boldsymbol{\Omega}_l \widetilde{\boldsymbol{q}} \, dt + \frac{\sigma}{2} \sum_{j=1}^{3} \mathbf{B}_j \widetilde{\boldsymbol{q}} \, dW_j(t) \\ \widetilde{\boldsymbol{q}}(0) &= \boldsymbol{q}^{(0)} \quad \text{s.t.} \quad \|\boldsymbol{q}^{(0)}\| = 1 \end{aligned} \tag{3.11}$$

As we are interested in the cumulative effect of measurement noise over time, we do not include an error for the initial value. The matrices $\mathbf{B}_j$ correspond to the imaginary units of the quaternions expressed as a subspace of $\mathbb{R}^{4\times 4}$

$$\mathbf{B}_1 = \begin{bmatrix} 0 & -1 & 0 & 0 \\ 1 & 0 & 0 & 0 \\ 0 & 0 & 0 & 1 \\ 0 & 0 & -1 & 0 \end{bmatrix} \qquad \mathbf{B}_2 = \begin{bmatrix} 0 & 0 & -1 & 0 \\ 0 & 0 & 0 & -1 \\ 1 & 0 & 0 & 0 \\ 0 & 1 & 0 & 0 \end{bmatrix}$$
$$\mathbf{B}_3 = \begin{bmatrix} 0 & 0 & 0 & -1 \\ 0 & 0 & 1 & 0 \\ 0 & -1 & 0 & 0 \\ 1 & 0 & 0 & 0 \end{bmatrix} \tag{3.12}$$

The matrices $\boldsymbol{\Omega}_l$ and $\mathbf{B}_j$ do not commute under multiplication, so there is no simple closed form solution for (3.11). To obtain a qualitative understanding of the error dynamics, we consider the simpler problem

$$d\widetilde{\boldsymbol{q}} = \frac{\sigma}{2}\mathbf{B}_j \widetilde{\boldsymbol{q}} \, dW_j(t) \qquad \widetilde{\boldsymbol{q}}(0) = \boldsymbol{q}^{(0)} \quad \text{s.t.} \quad \|\boldsymbol{q}^{(0)}\| = 1 \tag{3.13}$$

with no actual rotation and a single perturbed measurement. The unique solution is

$$\begin{aligned} \widetilde{\boldsymbol{q}} &= \exp\Big[\frac{\sigma}{2}\mathbf{B}_j W_j(t) - \frac{1}{2}\Big(\frac{\sigma}{2}\mathbf{B}_j\Big)^2 t\Big]\boldsymbol{q}^{(0)} = \\ &= \exp\Big(\frac{\sigma^2 t}{8}\Big)\Big[\cos\Big(\frac{\sigma}{2}W_j(t)\Big)\mathbf{I}_4 + \sin\Big(\frac{\sigma}{2}W_j(t)\Big)\mathbf{B}_j\Big]\boldsymbol{q}^{(0)} \end{aligned} \tag{3.14}$$

Here, we use the fact that $\mathbf{B}_j$ and $\mathbf{I}_4$ commute, as well as the properties

$$\mathbf{B}_j^2 = -\mathbf{I}_4 \qquad \exp(\lambda \mathbf{B}_j) = \cos(\lambda)\mathbf{I}_4 + \sin(\lambda)\mathbf{B}_j \tag{3.15}$$

Note that the norm of $\boldsymbol{q}$ grows at an exponential rate although the exact solution always satisfies $\|\boldsymbol{q}(t)\| = 1$. This is a property of the Itô integral which is replicated if we solve the SDE using the explicit Euler scheme. As we are only interested in the angles, the result is still useful if we normalise q before calculating the rotation matrix. A more satisfying solution would be to use an integration scheme that treats (3.13) as an SDE in the sense of Stratonovich, as the corresponding solution omits the growth term. However, the usual situation in practice is that neither the ODE nor the solver permit the analysis of error propagation in terms of a simple SDE. The recommended approach in this case is a Monte-Carlo study.

After we normalise the solution to the quaternion equation, its position on the unit sphere is still perturbed by the measurement noise. To see what this means in terms of the rotation matrix $\mathbf{S}$, we first consider the case that $j = 1$ and $\boldsymbol{q}^{(0)}$ is equal to the first unit vector. Equation (3.7) now yields the following result for $\theta(t) := \sigma W_1(t)/2$

$$\boldsymbol{q}(t) = \begin{bmatrix} \cos\theta(t) \\ \sin\theta(t) \\ 0 \\ 0 \end{bmatrix} \Rightarrow \mathbf{S} = \begin{bmatrix} 1 & 0 & 0 \\ 0 & \cos 2\theta(t) & -\sin 2\theta(t) \\ 0 & \sin 2\theta(t) & \cos 2\theta(t) \end{bmatrix} \tag{3.16}$$

This is a rotation around the x-axis, where the angle behaves like a Brownian motion, so its standard deviation is $O(t^{\frac{1}{2}})$, which we might expect for a single integration step. Analogous calculations for other values of j and i show that distorting (only) $\omega_{l,1}$ always results in a spurious rotation around the x-axis, while $\omega_{l,2}$ affects the y-axis, and $\omega_{l,3}$ the z-axis. We cannot provide an exact solution in the case of three noise terms and non-zero excitation, but the best we may expect are the errors growing at the same rate. Thus, including an INS in the process does not solve the problem of noisy data in general. However, short simulations can be stabilised using angular velocities measurements that are sufficiently accurate.

In practice, the accuracy of an INS is affected by other factors besides random noise. For short-term stability, manufacturers often express the standard deviation as being linear in operation time (a more detailed analysis may distinguish bias instability of $O(t)$ and angle random walk of $O(t^{\frac{1}{2}})$). The magnitude of these effects can range from below $0.001°$ per hour for high-performance INS used in aeronautics to over $10°$ per hour for the cheapest

units (Titterton and Weston, 2004). To choose the right measuring equipment for a task, one has to know the length of the individual measurements as well as the sensitivity of the vehicle model to deviations from the true angle. Even an error of $10°$ per hour can be acceptable for simulating a 5 minute drive.

As the final example, we consider a 10 minute segment of INS data recorded at a frequency of $1000\,\mathrm{Hz}$ ($\Delta t = 0.001\,\mathrm{s}$) on board a moving vehicle. Angular velocities were reconstructed by smoothing with a low-pass filter and taking central differences. For the purpose of demonstration, these will be treated as the 'true' values. The angles were reconstructed by solving quaternion equation (3.7) with added noise using the DOPRI(4,5) scheme (Dormand and Prince, 1980). For the errors, we used independent Gaussian random variables with mean zero and standard deviation $\sigma_M = 0.1$ radians per second. Taking (2.5) as a simple approximation, we expect that the angles behave similar to Brownian motion with standard deviation $\sigma = \frac{180°}{\pi}\sigma_M\sqrt{\Delta t} = 0.18\frac{°}{\sqrt{\mathrm{s}}}$. As the plots in Figs. 1 and 2 show, the errors are indeed of comparable magnitude.

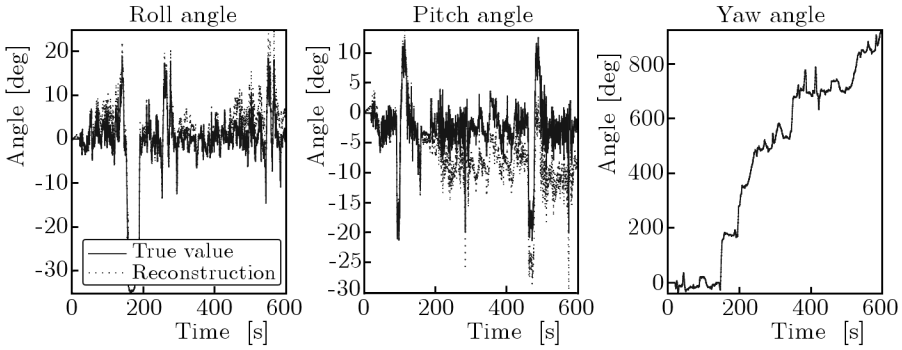

Fig. 1. True and reconstructed angles

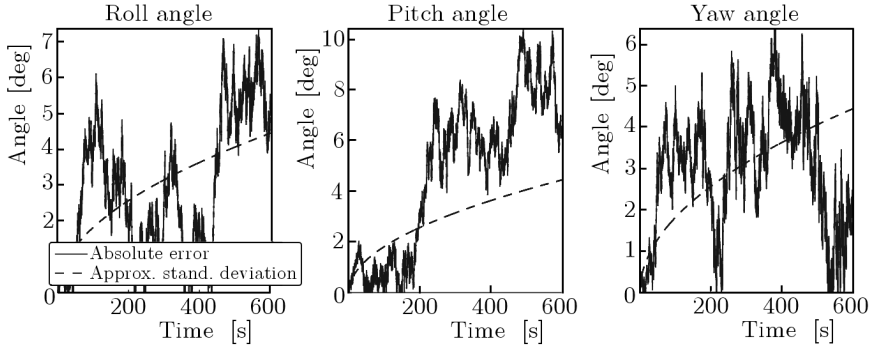

Fig. 2. Reconstruction error for angles

3.3. Stabilising the force-based simulation

In the preceding two sections, we have presented how to use additional measurements in order to approximately derive the true trajectory of a certain reference point of the vehicle body. Now, the vehicle motion in the force-based simulation can be stabilised by additionally prescribing the measured motion at the reference point. However, the enforced motion induces reaction forces given by the corresponding Lagrange multipliers. In an ideal situation with no noise in the measured data and a "perfect" model, these reaction forces should be zero.

There is a certain similarity to the Gear-Gupta-Leimkuhler stabilisation for the index reduced formulations of multibody equations (see Gear *et al.*, 1985). The idea of index reduction is to use constraints on the velocity or acceleration level in order to reduce the index of the DAE. But this leads to the well-known drift effect during integration of index 2 or index 1 formulations. This drift can be corrected either by projecting onto the known constraints on the position level or by using constraints both on the position as well as on the velocity or acceleration level. To compensate the additional constraints in the latter case, Gear, Gupta, and Leimkuhler introduced corresponding Lagrange multipliers η to the kinematic equation $\dot{\boldsymbol{x}} = \boldsymbol{v} - \boldsymbol{G}^{\top}(\boldsymbol{x})\eta$. In contrast to our case, no additional forces are introduced by that approach.

Since we are transferring data measured on a real vehicle to a numerical model, the reaction forces observed at the point of the prescribed motion are not only due to the noise in the wheel forces but also due to the fact that the numerical model is only an approximation of the real vehicle. While for the real vehicle the measured prescribed motion is 'in equilibrium' with the measured wheel forces (up to measurement noise), this need not be true for the numerical model. If, for example, the weight of the vehicle model is too small, then the vertical reaction force will show an offset which is needed to prevent the vehicle model from lifting off during simulation.

If the stabilised simulation is used, one has to check subsequently the magnitude of the artificial reaction forces in order to decide whether the approach is valid (small reaction forces) or not. Of course, in the latter case, it is in general not easy to find out the reason for the mismatch.

4. A simple example

We want to illustrate the considerations above using the vehicle model shown in Fig. 3. It is taken from Popp and Schiehlen (2008) and simple enough to write down the equations of motion explicitly and nevertheless useful for de-

monstrating the drift effects. The model contains three bodies (the chassis and two wheels) as well as two spring damper systems between the wheels and

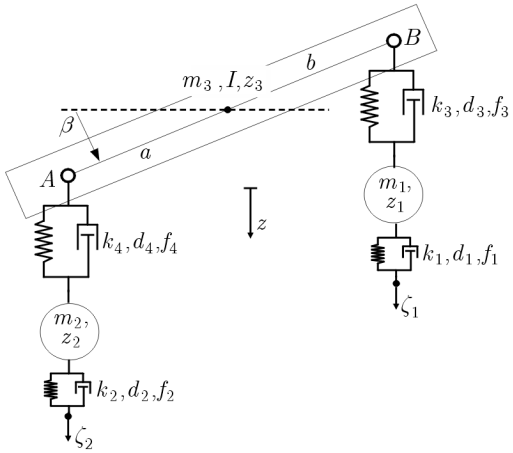

Fig. 3. A simple vehicle model

the chassis and two additional spring damper systems representing the tyres. The connection between the springs and the chassis is via revolute joints. The chassis moves in the vertical direction z_3 (positive z oriented downward) and rotates about the angle β (I denotes the moment of inertia of the chassis). The degrees of freedom of the wheels are z_1, z_2 resp. Thus, the entire system has six degrees of freedom, namely the coordinates of the three bodies z_1, z_2, z_3, β and the coordinates ζ_1, ζ_2 of the contact points to the ground. Details of the model can be found in App. 5.

4.1. Excitation modes of the model

The system may be excited by prescribing either (i) the vertical forces f_1, f_2 at the contact points, (ii) the road profile given by ζ_1, ζ_2, or (iii) the vertical forces f_1, f_2 and the pitch angle β. In the first case, the equations of motion may be written in the form

$$\mathbf{M}\dot{\boldsymbol{x}} = \mathbf{A}(\boldsymbol{x})\boldsymbol{x} + \boldsymbol{F} \tag{4.1}$$

where the vector of unknowns $\boldsymbol{x}$ is given by $\boldsymbol{x} = [z_1, z_2, z_3, \beta, \dot{z}_1, \dot{z}_2, \dot{z}_3, \dot{\beta}, \zeta_1, \zeta_2]^\top$ and the mass matrix $\mathbf{M}$ as well as the system matrix $\mathbf{A}(\boldsymbol{x})$ and the right hand side $\boldsymbol{F}$ are given in App. 5. In the second case, the forces f_1, f_2 at the contact points are reaction forces which are unknown and have to be calculated. The dynamic equations are now given by

$$\overline{\mathbf{M}}\dot{\overline{\boldsymbol{x}}} = \overline{\mathbf{A}}(\overline{\boldsymbol{x}})\overline{\boldsymbol{x}} + \overline{\boldsymbol{F}} \tag{4.2}$$

where the vector of unknowns is given by $\overline{\boldsymbol{x}} = [z_1, z_2, z_3, \beta, \dot{z}_1, \dot{z}_2, \dot{z}_3, \dot{\beta}]^\top$, and the mass matrix $\overline{\mathbf{M}}$ as well as the system matrix $\overline{\mathbf{A}}(\overline{\boldsymbol{x}})$ and the right hand side $\overline{\boldsymbol{F}}$ are given in App. 5. After solving these equations for $\overline{\boldsymbol{x}}$, we get the contact forces by

$$\begin{aligned} f_1 &= k_1(\overline{x}_1 - \zeta_1) + d_1(\overline{x}_5 - \dot{\zeta}_1) \\ f_2 &= k_2(\overline{x}_2 - \zeta_2) + d_2(\overline{x}_6 - \dot{\zeta}_2) \end{aligned} \tag{4.3}$$

In the third case, we stabilise the force-based simulation using the measured pitch angle. Here the vector of unknowns is $\widehat{\boldsymbol{x}} = [z_1, z_2, z_3, \dot{z}_1, \dot{z}_2, \dot{z}_3, \zeta_1, \zeta_2]^\top$ and the equations of motion are

$$\widehat{\mathbf{M}}\dot{\widehat{\boldsymbol{x}}} = \widehat{\mathbf{A}}\widehat{\boldsymbol{x}} + \widehat{\boldsymbol{F}} \tag{4.4}$$

The mass matrix $\widehat{\mathbf{M}}$, the system matrix $\widehat{\mathbf{A}}$, and the right side $\widehat{\boldsymbol{F}}$ are given in the appendix. The prescription of the angle β induces an enforced moment λ at the chassis center. Once the equations of motion have been solved, λ can be calculated by

$$\lambda = I\ddot{\beta} - \cos\beta(bf_3 - af_4)$$

where f_3, f_4 are the chassis spring forces defined in Appendix, Eqs. (A.1).
We now use the model to illustrate what may happen if wheel forces measured at a prototype vehicle on a certain track are used for exciting a numerical model (MBS) of the vehicle. Here, we have to replace the measurement by a first simulation of the model based on a predefined road profile ζ_1, ζ_2. The following steps are performed:

1. We simulate the model based on a prescribed road profile. The equations of motion are given by (4.2). Results are the vertical wheel forces which we denote by $f_1^{(0)}$, $f_2^{(0)}$. This step is called **virtual measurement**.
2. We simulate the model using (4.1), where $f_1 = f_1^{(0)}$ and $f_2 = f_2^{(0)}$. This step is called **simulation based on undisturbed forces**. In the absence of noise and calculation errors, we should get the same vehicle motion as in the virtual measurement.
3. We pretend a **measurement error** by adding a synthetic noise $\varepsilon_1, \varepsilon_2$ to the forces $f_1^{(0)}, f_2^{(0)}$. The noise is stationary with zero mean and variance σ^2. Then, we simulate the model using (4.1), where $f_1 = f_1^{(0)} + \varepsilon_1$ and $f_2 = f_2^{(0)} + \varepsilon_2$. This step is called **simulation based on noisy forces**.
4. We pretend a **modelling error** by slightly changing the stiffness and damping parameters k_3, d_3, k_4, d_4 of the chassis springs as well as the

moment of inertia I of the chassis. Then, we simulate the modified model using (4.1) with the unperturbed forces $f_1^{(0)}$, $f_2^{(0)}$. This step is called **simulation of a perturbed model**. Again we compare the corresponding vehicle motion with the motion from the virtual measurement.

5. We assume, that we have measured the pitch angle β and simulate the perturbed model with the noisy forces under prescription of β using (4.4). This step is called **stabilised simulation of the perturbed model**.

4.2. Simulation results

The road profile and the wheel forces

In Fig. 4, the road profile used for the virtual measurement and the resulting wheel forces are shown. The profile starts at level zero and ranges

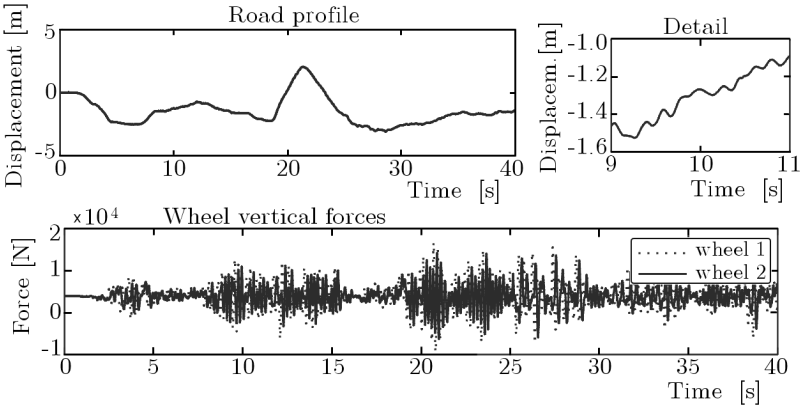

Fig. 4. The basic road profile ζ_1, ζ_2 at the top and the resulting wheel forces at the bottom

approximately between $-2\,\mathrm{m}$ and $+2\,\mathrm{m}$, simulating some small hill grades. The resulting vertical wheel forces are shown below. They are rather similar for both wheels. Their amplitudes (approximately between $-10\,\mathrm{kN}$ and $+16\,\mathrm{kN}$) are due to the road roughness which can be seen in a detail plot of the profile.

Noisy forces and perturbed models

As a model for the measurement error of the forces, we have used Gaussian white noise signals ε_1, ε_2 with standard deviation $\sigma = 0.002 f_{max}$, where f_{max} is the maximum absolute force. Thus, we get $\sigma \approx 32\,\mathrm{N}$.

When comparing the simulation results with the virtual measurement, we only show the vertical chassis motion z_3 and the pitch angle β. The latter is the most sensitive variable. The differences in z_1 and z_2 are smaller in most cases. The virtual measurement is compared to the simulation with undisturbed forces, to the simulation with noisy forces, and to the simulation with the perturbed model. Figure 5 shows the results for the vertical chassis motion

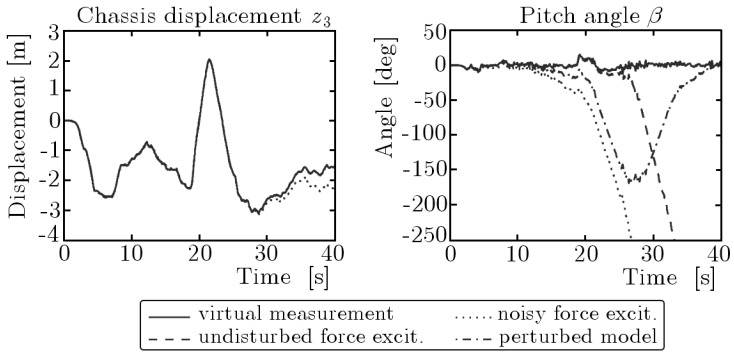

Fig. 5. Vertical chassis motion z_3 and the pitch angle β during different simulations

(left) as well as for the pitch angle (right). There is nearly no drift in z_3 with the exception of the noisy force excitation, where a relatively small drift can be observed. For the pitch angle, we observe a drift beyond 20 s even for the simulation with undisturbed forces. As can be expected, the drift-off occurs much earlier (at 10 s approximately) in the case of noisy forces or the perturbed model.

In Fig. 6 and Fig. 7, the results for different noise samples and different perturbed models resp. are shown. While the behaviour of the different noisy force results is fairly similar with respect to the "drift-off" time, the specific

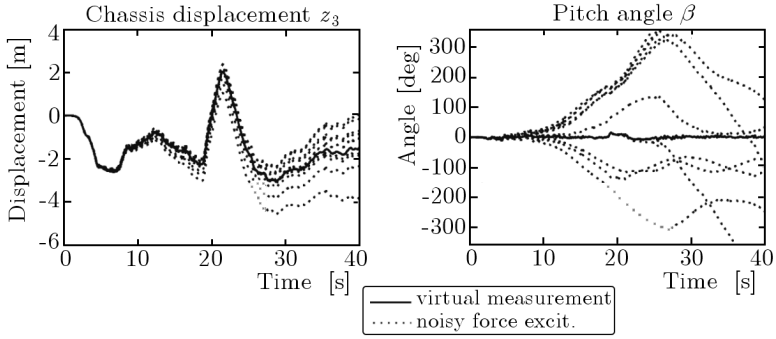

Fig. 6. Vertical displacement (left) and the pitch angle β (right) of the chassis during force-based excitation for several samples of the noise

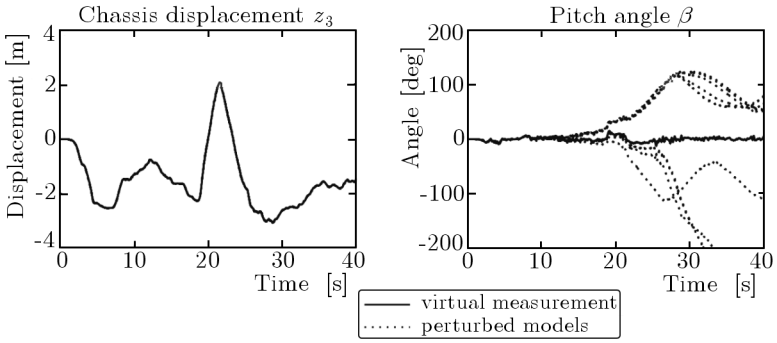

Fig. 7. Vertical displacement (left) and the pitch angle β (right) of the chassis during force-based excitation for several perturbed models. The perturbation is a random factor between 0.9 and 1.1 (at most 10%) on the stiffness and damping parameters of the chassis springs and on the moment of inertia of the chassis

trajectories differ a lot. This is in accordance with what can be observed for multiple paths of the simple point mass example in Sec. 2. In the case of the perturbed model, we observe nearly no drift in the vertical chassis displacement and different types of drifts for the pitch angle depending on the specific way, the perturbed model parameters are affecting the physical behaviour.

Prescription of the pitch angle

Next we study the effect of prescribing the pitch angle β (stabilisation). When simulating the original model with presribed β and undisturbed forces, we get a small enforced moment (not shown) due to small numerical integration errors. In that case its magnitude is approximately 70 Nm. If we do the same for the perturbed model and the noisy forces, we have to expect a larger moment. In Fig. 8, the results from the stabilised simulation of the perturbed model excited by the noisy forces are shown. The plot shows the enforced moment (right) and compares it to the inertia term $I\beta$ (left). The enforced moment approximately ranges between $(-800\,\mathrm{Nm}, 800\,\mathrm{Nm})$ which is considerably larger than in the case without the model and force error. However, if we compare the magnitude of the enforced moment with the magnitude of the inertia term $I\beta$, which approximately is 15 kNm, we find that it is relatively small.

The magnitude of the moment can be regarded as a measure of inconsistency between the applied forces, the model, and the enforced motion β. Thus, it should be as small as possible. Of course, in practice it is not known, whether the enforced moment is mainly due to erroneous forces, model errors, or an erroneous prescribed motion.

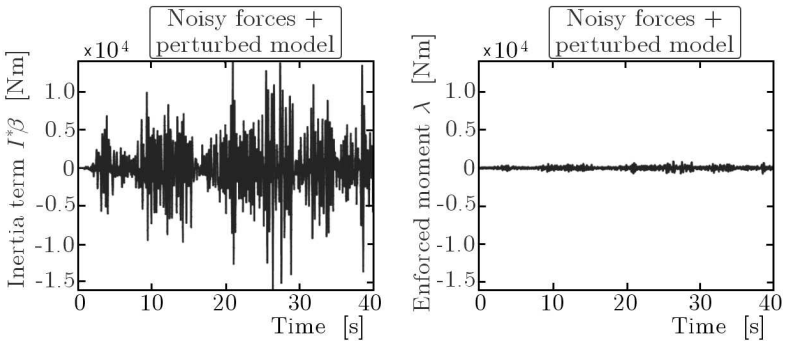

Fig. 8. The inertia term $I\beta$ (left) and the moment enforced by the prescription of the pitch angle (right)

Remark

For the calculations above, the equations of motion given in the appendix have been implemented in MATLAB and solved with different integration schemes (ode45: a Runge-Kutta method by Dormand and Prince (1980), ode113: a variable order Adams-Bashforth-Moulton method, see Shampine and Gordon (1975), ode15s: a variable order solver based on numerical differentiation formulas (NDFs), see Shampine and Reichelt (1997)) and different error tolerances ($tol_{rel} \in \{10^{-4}, 10^{-8}\},\ tol_{abs} \in \{10^{-6}, 10^{-10}\}$). It turned out that the presence of the observed drift is essentially independent of the solver and the accuracy of the integration.

5. Conclusions

Starting with the theory of stochastic differential equations, we argued that the drift effect during force-based simulation of unconstrained models cannot be eliminated by suitable integration schemes. It is a consequence of noise in the excitation data. In addition, the integration errors, although controlled by tolerances, may accumulate as has been described in Sec. 2. This can be compared to the well known drift-off of DAE solutions using index 1 or 2 formulations. However, in those cases, we can apply stabilisation techniques (e.g. Baumgarte stabilisation, see Baumgarte (1972)) since we know the constraints at the position level as well. See Ascher and Petzold (1998), Brenan *et al.* (1996), or Eich-Soellner and Führer (1998) for details on ODE and DAE solving.

As we do not know the true trajectory, such techniques do not help here. The only way around that problem is to stabilise the simulation (Sec. 3.3) making use of data on the position level. Since a pure translational drift does not affect section forces, we can concentrate on controlling the orientation.

As we have seen in Sec. 3.1, we can calculate the orientation from measured accelerations, but during that twofold integration process, we again have the drift problem. Using suitable measurement equipment, we can obtain the angular velocities such that we have to perform only one integration leading to a much smaller drift. It is now a matter of the quality of the measurement equipment to keep the errors sufficiently small. Some of the measurement devices internally perform that integration step and deliver the orientation angles directly. For more details see Sec. 3.2 and the references therein. Finally, in Sec. 4, a simple example has been used to illustrate the considerations.

Appendix A: The equations of motion of the vehicle model

In the following, the equations of motion of the system are derived (see Fig. 3 for notation). We start with the spring forces given by Hook's law and a viscous damping term and the force equilibrium

$$\begin{aligned} f_i &= k_i(z_i - \zeta_i) + d_i(\dot{z}_i - \dot{\zeta}_i) \qquad i = 1,2 \\ f_3 &= k_3(z_3 - z_1 - b\sin\beta) + d_3(\dot{z}_3 - \dot{z}_1 - b\dot{\beta}\cos\beta) \\ f_4 &= k_4(z_3 - z_2 + a\sin\beta) + d_4(\dot{z}_3 - \dot{z}_2 + a\dot{\beta}\cos\beta) \end{aligned} \tag{A.1}$$

and

$$\begin{aligned} m_1\ddot{z}_1 &= m_1 g + f_3 - f_1 & m_2\ddot{z}_2 &= m_2 g + f_4 - f_2 \\ m_3\ddot{z}_3 &= m_3 g - f_3 - f_4 & I\ddot{\beta} &= \cos\beta(bf_3 - af_4) \end{aligned} \tag{A.2}$$

Force excitation

Introducing $\boldsymbol{x} = [z_1, z_2, z_3, \beta, \dot{z}_1, \dot{z}_2, \dot{z}_3, \dot{\beta}, \zeta_1, \zeta_2]^\top$, combining (A.1), (A.2) and using the abbreviations $c_4 = \cos x_4$, $s_4 = (\sin x_4)/x_4$ results in the following equations

$$\mathbf{M}\dot{\boldsymbol{x}} = \mathbf{A}(\boldsymbol{x})\boldsymbol{x} + \boldsymbol{F} \qquad \mathbf{M} = \operatorname{diag}(1,1,1,1,m_1,m_2,m_3,I,d_1,d_2)$$

$$\boldsymbol{F} = [0,0,0,0,m_1 g - f_1, m_2 g - f_2, m_3 g, 0, -f_1, -f_2]^\top$$

$$\mathbf{A} = \begin{bmatrix} \mathbf{0} & \mathbf{I}_4 & \mathbf{0} \\ \mathbf{A}_{21} & \mathbf{A}_{22} & \mathbf{0} \\ \mathbf{A}_{31} & \mathbf{A}_{32} & \mathbf{A}_{33} \end{bmatrix}$$

$$\mathbf{A}_{21} = \begin{bmatrix} -k_3 & 0 & k_3 & -bk_3 s_4 \\ 0 & -k_4 & k_4 & ak_4 s_4 \\ k_3 & k_4 & -k_3 - k_4 & (bk_3 - ak_4)s_4 \\ -bk_3 c_4 & ak_4 c_4 & (bk_3 - ak_4)c_4 & (-b^2 k_3 - a^2 k_4)c_4 s_4 \end{bmatrix} \tag{A.3}$$

$$\mathbf{A}_{22} = \begin{bmatrix} -d_3 & 0 & d_3 & -bd_3 c_4 \\ 0 & -d_4 & d_4 & ad_4 c_4 \\ d_3 & d_4 & -d_3 - d_4 & (bd_3 - ad_4)c_4 \\ -bd_3 c_4 & ad_4 c_4 & (bd_3 - ad_4)c_4 & (-b^2 d_3 - a^2 d_4)c_4^2 \end{bmatrix}$$

$$\mathbf{A}_{31} = \begin{bmatrix} k_1 & 0 & 0 & 0 \\ 0 & k_2 & 0 & 0 \end{bmatrix} \qquad \mathbf{A}_{32} = \begin{bmatrix} d_1 & 0 & 0 & 0 \\ 0 & d_2 & 0 & 0 \end{bmatrix}$$

$$\mathbf{A}_{33} = -\begin{bmatrix} k_1 & 0 \\ 0 & k_2 \end{bmatrix}$$

Equation (A.3) describes the system excited by the forces f_1, f_2 at the contact points to the ground. The system matrix $\mathbf{A}(\boldsymbol{x})$ depends on the pitch angle only ($\mathbf{A}(\boldsymbol{x}) = \mathbf{A}(\boldsymbol{x}_4) = \mathbf{A}(\beta)$). For small angles β we have $\cos\beta \approx 1$ and $(\sin\beta)/\beta \approx 1$ such that the vehicle can be described by a linear system $\mathbf{M}\dot{\boldsymbol{x}} = \mathbf{A}(0)\boldsymbol{x} + \boldsymbol{F}$.

Excitation by a road profile

If the system is excited by a given road profile ζ_1, ζ_2, then the forces f_1, f_2 at the contact points are reaction forces which are unknown prior to simulation. In that case the dynamic equations are given by

$$\begin{aligned} &\overline{\mathbf{M}}\dot{\overline{\boldsymbol{x}}} = \overline{\mathbf{A}}(\overline{\boldsymbol{x}})\overline{\boldsymbol{x}} + \overline{\boldsymbol{F}} \qquad \overline{\mathbf{M}} = \operatorname{diag}(1,1,1,1,m_1,m_2,m_3,I) \\ &\overline{\boldsymbol{F}} = [0,0,0,0,m_1 g + k_1\zeta_1 + d_1\dot{\zeta}_1, m_2 g + k_2\zeta_2 + d_2\dot{\zeta}_2, m_3 g, 0]^\top \\ &\overline{\mathbf{A}} = \begin{bmatrix} \mathbf{0} & \mathbf{I}_4 \\ \overline{\mathbf{A}}_{21} & \overline{\mathbf{A}}_{22} \end{bmatrix} \\ &\overline{\mathbf{A}}_{21} = \mathbf{A}_{21} - \begin{bmatrix} k_1 & 0 & 0 & 0 \\ 0 & k_2 & 0 & 0 \\ 0 & 0 & 0 & 0 \\ 0 & 0 & 0 & 0 \end{bmatrix} \\ &\overline{\mathbf{A}}_{22} = \mathbf{A}_{22} - \begin{bmatrix} d_1 & 0 & 0 & 0 \\ 0 & d_2 & 0 & 0 \\ 0 & 0 & 0 & 0 \\ 0 & 0 & 0 & 0 \end{bmatrix} \end{aligned} \tag{A.4}$$

where the vector of unknowns $\overline{\boldsymbol{x}}$ is given by $\overline{\boldsymbol{x}} = [z_1, z_2, z_3, \beta, \dot{z}_1, \dot{z}_2, \dot{z}_3, \dot{\beta}]^\top$.

Force excitation with a prescribed pitch angle

If we prescribe the pitch angle β during force excitation f_1, f_2, we get an enforced moment λ at the center of mass of body 3. Since β is no longer an unknown, we

introduce the new variable vector $\widehat{\boldsymbol{x}} = [z_1, z_2, z_3, \dot{z}_1, \dot{z}_2, \dot{z}_3, \zeta_1, \zeta_2]^\top$. Skipping the β-rows of the matrix $\mathbf{A}(\boldsymbol{x})$ in (A.3) and putting the β-columns into the new force vector $\widehat{\boldsymbol{F}}$ leads to

$$\widehat{\mathbf{M}}\dot{\widehat{\boldsymbol{x}}} = \widehat{\mathbf{A}}\widehat{\boldsymbol{x}} + \widehat{\boldsymbol{F}} \qquad \widehat{\mathbf{M}} = \operatorname{diag}(1, 1, 1, m_1, m_2, m_3, d_1, d_2)$$

$$\widehat{\boldsymbol{F}} = \begin{bmatrix} 0 \\ 0 \\ 0 \\ m_1 g - f_1 - k_3 b \sin\beta - d_3 b \dot{\beta} \cos\beta \\ m_2 g - f_2 + k_4 a \sin\beta + d_4 a \dot{\beta} \cos\beta \\ m_3 g + (k_3 b - k_4 a) \sin\beta + (d_3 b - d_4 a) \dot{\beta} \cos\beta \\ -f_1 \\ -f_2 \end{bmatrix} \tag{A.5}$$

$$\widehat{\mathbf{A}} = \begin{bmatrix} 0 & 0 & 0 & 1 & 0 & 0 & 0 & 0 \\ 0 & 0 & 0 & 0 & 1 & 0 & 0 & 0 \\ 0 & 0 & 0 & 0 & 0 & 1 & 0 & 0 \\ -k_3 & 0 & k_3 & -d_3 & 0 & d_3 & 0 & 0 \\ 0 & -k_4 & k_4 & 0 & -d_4 & d_4 & 0 & 0 \\ k_3 & k_4 & -k_3 - k_4 & d_3 & d_4 & -d_3 - d_4 & 0 & 0 \\ k_1 & 0 & 0 & d_1 & 0 & 0 & -k_1 & 0 \\ 0 & k_2 & 0 & 0 & d_2 & 0 & 0 & -k_2 \end{bmatrix}$$

The system matrix $\widehat{\mathbf{A}}$ does no longer depend on the unknown states $\widehat{x}$. Thus, the vehicle excited by the contact forces and guided by the prescription of β is represented by a linear model.

Model parameters

The following parameters are used:

geometry [m]	inertia	stiffness [N/m]	damping [Ns/m]
$a = 1$	$m_1 = 15\,\mathrm{kg}$	$k_1 = 2 \cdot 10^5$	$d_1 = 2 \cdot 10^2$
$b = 1$	$m_2 = 15\,\mathrm{kg}$	$k_2 = 2 \cdot 10^5$	$d_2 = 2 \cdot 10^2$
	$m_3 = 750\,\mathrm{kg}$	$k_3 = 1 \cdot 10^5$	$d_3 = 1 \cdot 10^4$
	$I = 500\,\mathrm{kgm}^2$	$k_4 = 1 \cdot 10^5$	$d_4 = 1 \cdot 10^4$

For the perturbed model, the stiffness and damping of the chassis springs as well as the moment of inertia of the chassis have been changed according to

$$k_3 \leftarrow k_3 \cdot 1.05 \qquad k_4 \leftarrow k_4 \cdot 0.95 \qquad d_3 \leftarrow d_3 \cdot 0.95$$
$$d_4 \leftarrow d_4 \cdot 1.05 \qquad I \leftarrow I \cdot 0.95$$

References

1. ASCHER U., PETZOLD L.R., *Computer Methods for Ordinary Differential Equations and Differential-Algebraic Equations*, SIAM, Philadelphia
2. BAUMGARTE J., 1972, Stabilization of constraints and integrals of motion in dynamical systems, *Comp. Methods Appl. Mech.*, **1**, 1-16
3. BRENAN K.E., CAMPBELL S.L., PETZOLD L.R., 1996, *Numerical Solution of Initial-Value Problems in Differential-Algebraic Equations*, SIAM, Philadelphia, 2nd edition
4. DORMAND J.R., PRINCE P.J., 1980, A family of embedded Runge-Kutta formulae, *J. Comp. Appl. Math.*, **6**, 19-26
5. EICH-SOELLNER E., FÜHRER C., 1998, *Numerical Methods in Multibody Dynamics*, Teubner-Verlag, Stuttgart
6. GEAR C.W., GUPTA G.K., LEIMKUHLER B.J., 1985, Automatic integration of the Euler-Lagrange equations with constraints, *J. Comp. Appl. Math.*, **12/13**, 77-90
7. KLOEDEN P.E., PLATEN E., SCHURZ H., 2002, *Numerical Solution of SDE Through Computer Experiments*, Springer-Verlag Series Universitext
8. POPP K., SCHIEHLEN W., 2008, *Ground Vehicle Dynamics – A System Dynamics Approach*, Springer-Verlag Berlin
9. SHAMPINE L.F., GORDON M.K., 1975, *Computer Solution of Ordinary Differential Equations: the Initial Value Problem*, W.H. Freeman, SanFrancisco
10. SHAMPINE L.F., REICHELT M.W., 1997, The MATLAB ODE Suite, *SIAM Journal on Scientific Computing*, **18**, 1-22
11. TITTERTON D.H., WESTON J.L., 2004, *Strapdown Inertial Navigation Technology*, The Institution of Electrical Engineers

Efekt niestabilności numerycznej wielobryłowego modelu pojazdu przy wymuszeniu zadanym przyspieszeniami lub siłami wziętymi z pomiarów

Streszczenie

W przemyśle samochodowym bardzo istotną rolę pełnią symulacje numeryczne wielobryłowych modeli kompletnych pojazdów, wykonywane na podstawie pomiarów sił i momentów działających na koła, w celu późniejszego obliczania sił wewnętrznych w przekrojach różnych elementów dla oceny ich wytrzymałości. Zadanie to jest dość trudne ze względu na szum danych wejściowych uzyskanych w drodze pomiarów oraz

nieuniknione rozbieżności w sformułowaniu modelu w stosunku do obiektu rzeczywistego. Obydwa te czynniki powodują niestabilność numeryczną modelu. Prezentowana praca opisuje pokrótce źródła tych efektów i pokazuje, że wskutek braku wiedzy na temat rzeczywistej trajektorii pojazdu, problem ten nie może być rozwiązany jedynie w drodze zastosowania bardziej wydajnych narzędzi całkowania numerycznego równań ruchu. Przedstawiono jednak kilka koncepcji wyjścia naprzeciw temu problemowi. Na koniec, opisano prosty model pojazdu odzwierciedlający wszystkie te zagadnienia.

Manuscript received November 30, 2009; accepted for print April 12, 2010